We are IntechOpen, the world's leading publisher of Open Access books Built by scientists, for scientists

4,800
Open access books available

122,000
International authors and editors

135M
Downloads

Our authors are among the

154
Countries delivered to

TOP 1%
most cited scientists

12.2%
Contributors from top 500 universities

CLARIVATE ANALYTICS BOOK CITATION INDEX INDEXED

WEB OF SCIENCE™

Selection of our books indexed in the Book Citation Index in Web of Science™ Core Collection (BKCI)

Interested in publishing with us?
Contact book.department@intechopen.com

Numbers displayed above are based on latest data collected.
For more information visit www.intechopen.com

10

Electromagnetic Flow Metering

Jens Krause
FuE Zentrum FH Kiel GmbH, Kiel
Germany

1. Introduction

Numerical simulations have become an integral part of new sensor design and they are essential to understand the physical principles of completely new sensors. In this chapter we want to demonstrate that, when using modern software tools, relevant results are in reach even for small development departments.

The electromagnetic flow meter, that measures the volume flow rate of conducting liquids passing through pipes, is a very practical example for a sensor that is used in real applications, but that has still potential for improvement and optimisation by numerical simulations. The goal of this chapter is to show, in three concrete cases, different levels of modelling.

The chapter will introduce the concepts of electromagnetic flow metering and the physical phenomena needed for numerical modelling. The main goal is to show that physical principles can be studied with detail and that, nevertheless, calculations are relevant to practical applications.

We demonstrate the ideas in three detailed cases.

1. Until now, commercially available devices require a minimum conductivity of water, i.e., a minimum concentration of ions. Using numerical methods one can study the low concentration limit of the electromagnetic flow meter. The central idea is to apply a drift-diffusion model to the system of electric charges present in the fluid.
2. For standard devices several physical phenomena are encountered: fluid dynamics, magnetostatics, and electrostatics. We demonstrate the efficient use of multiphysics solvers for the geometric optimisation of a sensor. The geometric shape is optimised much easier numerically than it can be done in experiments.
3. A completely new sensor principle can be verified using numerical simulation for turbulent flows. By studying the amplitude of fluctuations we find a new way of measuring the mean flow, which is in accordance with experiments.

The numerical scheme for these calculations is based on finite methods: in many cases the very flexible finite element method can be employed. It can solve a wide range of physical problems and a large class of geometries. Standard software packages are available for all equations needed for flow sensor design. On the other hand the finite difference method requires regular grids but can, due to its inherent speed, solve large problems like the turbulent direct numerical simulation, where space and time must be resolved in a fine discretisation.

2. Magnetic-inductive flow meter

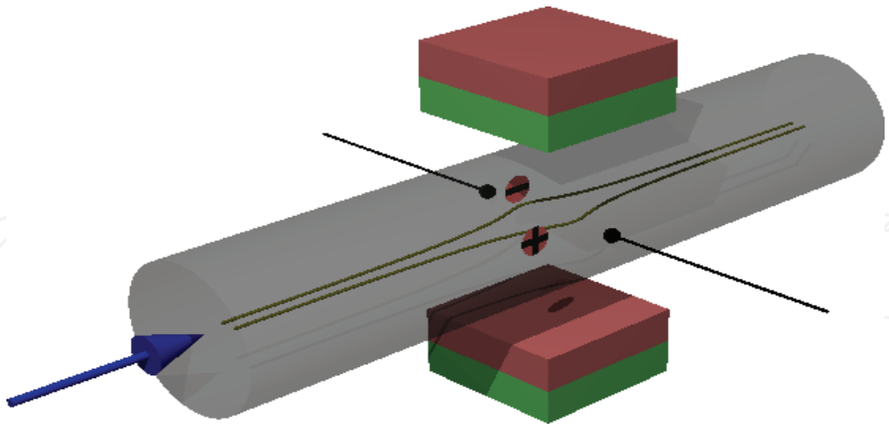

Figure 1. Principle of the electromagnetic flow meter. Ions are displaced by an outer magnetic field and a electric voltage can be measured at galvanic contacts (black circles)

The basic idea of the electromagnetic (or magnetic-inductive, MI) flow meter for measuring fluid flow in pipes shall be explained with the help of fig. 1. An external magnetic field perpendicularly penetrates the tube carrying fluid flow. If the fluid contains mobile electric charges these are displaced (with respect to the fluid) due to the Lorentz-force. The accumulated charges form a space charge density and an electric field is induced which prevents further charge separation. The electric potential can be sensed using galvanic or capacitive coupling. In ideal cases the measured voltage is proportional to the flow rate in the tube.

The idea of this method is old, if one considers Michael Faraday's famous experiment at the river Thames as a starting point. Later, in 1930, Williams reported the first experimental proof (Williams 1930) and today the MI-flow meter has become a commercial product used in many applications in industry: process, food, waste water, etc. The theory is mature and text books have been published that are entirely (Schommartz 1974) or in parts (Fiedler 1992) devoted to the subject.

The sensors are mainly employed for water as liquid, although the use for other electrically conducting fluids is feasible. Standard devices avoid permanent magnets because of spurious electrochemical voltages at the sensing contacts. Even with electrodes made of noble metals, chemical reactions are present in water at galvanic contacts and lead to time-varying electric potentials, that are larger than the actual MI-signal. By using alternating or pulsed magnetic fields these variations can be filtered. Capacitive coupling suffers from the difficulty to measure small charges when the inner resistance of the pick-up circuit is finite.

But the price for time varying magnetic fields is high energy consumption. Up to 99% of the total energy is spent on the generation of the magnetic field, which is prohibitive for battery driven devices. Using modern electronic devices with ultra-high-ohmic amplifiers, static measurements have become feasible and a recent patent (Stange 2002) describes a method to bypass spurious voltages. Therefore some aspects in the field of electromagnetic flow metering have to be rethought and can be studied using numerical simulations.

The Finite-Element method has become a versatile tool in solving partial differential equations (PDEs) in many scientific and engineering disciplines. Many text books describe the method in different aspects and we only want to cite one of the most influential by

Zienkiewicz (Zienkiewicz & Taylor 1989) first published on structural mechanics. Since then the method has been applied to other engineering fields and due to the increased computer power became available to developers for daily use.
For MI-sensors the literature using FE-simulation is sparse but many applications in industry are on optimising the coils generating the magnetic field. Here we focus on the study of fundamental physical understanding and geometric optimisation. Many publications on electromagnetic flow meters use the concept of a *weight function* to analyse the design. This concept will be mentioned briefly because it is widely used but it is restricted to the high concentration limit (that we want to study in detail) and to galvanic contacts concentrated in points.

3. Mathematical models

The different physical effects and their equations are discussed in the following with their relevance to the electromagnetic flow meter.

3.1 Fluid dynamics (Navier-Stokes equations)

The equations for fluid flow are derived from the basic physical principles of conservation of mass, of momentum, and of energy applied to continuum mechanics. Many text books on this subject, e.g., Spurk & Aksel (2006), are available and only basic properties are stated here without proofs.
Fluid flow is usually described by the Eulerian view, that represents the velocity of the fluid as vector field **u** at a fixed point in space. Two additional scalar fields are needed in general: the pressure p and the mass density ρ. In an incompressible fluid the system reduces to **u** and p and the incompressibility condition replaces the conservation of mass:

$$\nabla \cdot \mathbf{u} = 0 \,. \tag{1}$$

The conservation of momentum leads to

$$\rho \dot{\mathbf{u}} + \rho(\mathbf{u} \cdot \nabla)\mathbf{u} = -\nabla \mathrm{p} + \mu \Delta \mathbf{u} \,. \tag{2}$$

The left hand side represents the change of momentum in time at a fixed point in space. The right hand side denotes that the contributing forces are the pressure gradient as the driving force of the flow and the dissipative friction term. In the viscous model friction is caused by a velocity gradient and the proportionality constant μ is called viscosity. These equations are known as the incompressible Navier-Stokes (NS) equations. The boundary condition at physical walls is that the flow velocity is zero. Other mathematical boundary conditions are applied to inlets, outlets, and symmetry planes. The system of equation (1) and (2) is closed: it comprises four equations for four unknowns.

3.2 Magnetic inductive effect

The basic principle is that electric charges (like ions from dissolved salts) in the fluid are displaced due the Lorentz-force in response to an external magnetic field that is orthogonal to the fluid flow. The charge separation leads to an electric field **E** perpendicular both to the flow and the magnetic field. The electric potential φ can be sensed with galvanic contacts or with capacitive sensors.

In a conducting medium the electric current density $\mathbf{j}$ in presence of an electromagnetic fields is

$$\mathbf{j} = \sigma(\mathbf{E} + \mathbf{u} \times \mathbf{B}) \tag{3}$$

where σ is the specific conductivity. In an equilibrium state the current density is divergence free because of charge conservation and it follows that

$$\Delta\varphi = \nabla \cdot (\mathbf{u} \times \mathbf{B}) . \tag{4}$$

This equation has been cited in the literature (Shommartz 1974; Fiedler 1992) and is called here the *high concentration limit* and we discuss the validity of this model later. Here and in later models it is assumed that $\mathbf{B}$ is the external magnetic field only. The flowing medium itself drives electric currents which induce magnetic fields that are in the case of electrolytes too weak to have an influence. Two types of currents can be distinguished: The first one is generated by the charge density that is convected by the fluid, whereas the second one is the current as expressed in eq. (3).

The *weight function* approach applies Green's theorem to equation (4) and is often used to examine MI-flow meters. The Green's function that corresponds to the Laplace operator reads

$$G(x, x') = \frac{1}{4\pi|x - x'|} \tag{5}$$

and can be employed to express solutions of (4) as an integral. If two galvanic contacts are concentrated in points the voltage

$$\begin{aligned} V_{ab} &= \varphi(a) - \varphi(b) \\ &= -\int [\nabla_x G(a, x) - \nabla_x G(b, x)] \cdot (\mathbf{u} \times \mathbf{B}) d^3x \end{aligned} \tag{6}$$

is measured. The expression in square brackets is called the weight function $\mathbf{W}(a,b,x)$ (Shercliff 1954; Fiedler 1992). The integral can be transformed to

$$V_{ab} = \int \mathbf{u} \cdot (\mathbf{W} \times \mathbf{B}) d^3x . \tag{7}$$

In this form the integral formulation is helpful to design the magnetic field, e.g., to guarantee the property that the voltage is independent of flow profile. This approach is, however, limited to a simple governing equation and to pointlike galvanic contacts. Since more general problems must be solved we adopt the more flexible Finite-Element-Method.

3.3 Electrostatics and Magnetostatics

Maxwell's equations are only applied to the static field case only. In the macroscopic form, i.e., using material properties like permittivity, permeability, and magnetisation, the following equations are valid for the electric field:

$$\begin{aligned} \nabla \cdot (\varepsilon_0 \varepsilon_r \mathbf{E}) &= \rho \\ \mathbf{E} &= -\nabla\varphi \end{aligned} \tag{8}$$

where **E** is the electric field, φ the potential, ε_0 the permittivity of the vacuum and ε_r the relative permittivity of the material in question.
The relations for the fields **H** (magnetic field), **B** (magnetic induction), and **M** (magnetisation) are

$$\begin{aligned} \nabla \cdot \mathbf{B} &= 0 \\ \nabla \times \mathbf{H} &= 0 \\ \mathbf{B} &= \begin{cases} \mu_0 \mu_r \mathbf{H} \\ \mu_0 (\mathbf{H} + \mathbf{M}) \end{cases} \end{aligned} \tag{9}$$

The first material relationship is used for the usual linear response to a magnetic field, whilst the second is used as an approximation for permanent magnets with a given fixed magnetisation.
As mentioned above the magnetic fields produced by the currents in the medium are weak and these currents are altogether neglected as sources of the magnetic field. Since the curl of the magnetic field is zero under these circumstances a scalar magnetic potential with

$$\mathbf{H} = -\nabla \Theta \tag{10}$$

is introduced and used later for solving magnetostatic equations.

3.4 Drift-Diffusion

The evolution of the concentration c of an ion species in a medium is often described in electrochemistry (Hamann & Vielstich 2004) using the drift-diffusion approach. The effective current is generated in two ways: first, a driving force **F** on the individual particle and second the thermal diffusion. Applying Einstein's law we can write for each species

$$\mathbf{j} = \mu (c\mathbf{F} - k_B T \nabla c) \tag{11}$$

where μ is the mobility, k_B Boltzmann's constant and T the absolute temperature. We want to apply this model to diluted salts in water. For higher concentrations the linear mobility model is not valid, but here study only low concentration effects (Atkins 1988). The force **F** is due to an electrostatic field and to a magnetic induction

$$\mathbf{F} = q(\mathbf{E} + \mathbf{u} \times \mathbf{B}). \tag{12}$$

We only consider the Lorentz-force caused by the medium flow **u**, the additional velocity induced by the movement of ions with respect to the water is small and neglected in our model. The conservation of particle number is written as

$$\dot{c} + \nabla \cdot \mathbf{j} = G, \tag{13}$$

where the dot signifies the derivative with respect to time and G the particle generation rate. The boundary conditions are generally of the homogeneous Neumann-type for wall boundaries that the particles cannot penetrate. Often the total number of particles is fixed and an integral constraint in the form

$$\int c \, d^3x = N \tag{14}$$

is added to the equations. When multiple species are present the equations (11,12,13) have to be formulated for each type separately.

4. Finite-Element-Method

The finite element method is an established technique in academia and industry to approximately solve partial differential equations and applies to boundary value problems. Many authors (Zienkiewicz & Taylor 1989; Ciarlet 1978) have discussed the method in detail and for many applications.

One way of formulating boundary value problem, which is useful for many physical applications, is based on generalised sources and fluxes. For a degree of freedom u, the flux $\mathbf{J}$ and the source term S depend on u and its derivatives. The boundary value problem sets conditions on the inner of a domain Ω and on the boundary such that

$$\begin{aligned} \nabla \cdot \mathbf{J} &= \mathrm{S} \quad \text{in} \quad \Omega \\ \mathrm{u} &= \mathrm{f} \quad \text{in} \quad \Gamma_{\mathrm{D}} \subseteq \partial\Omega \\ \mathbf{n} \cdot \mathbf{J} &= \mathrm{g} \quad \text{in} \quad \Gamma_{\mathrm{N}} = \partial\Omega / \Gamma_{\mathrm{D}}. \end{aligned} \tag{15}$$

These equations imply the conservation of a quantity in the domain, Dirichlet condition (prescribed value f) on one part of the boundary, and Neumann condition (prescribed normal flux g) on the remaining boundary. In the case of a vectorial physical property or a multiphysics problem, several unknowns u_i have to be taken into account. For each unknown there is one set of equations in the form (15). If the generalised fluxes and sources depend mutually on each other the system is coupled.

The Finite-Element (FE) method approximates the solution by polynomial functions defined on elements (e.g. triangles or tetrahedrons), i.e., a continuous problem is projected on a discrete problem that can be solved on computers. A finite number of elements forms a conformal mesh of the domain thus leading to a finite number of degrees of freedom. Using the method of weighted residuals (Zienkiewicz & Taylor 1989) a discrete system with the same number of equations can be deduced from eq. (15). This system of equations is in general nonlinear and Newton's method is employed to find solutions. The resulting linear equations are sparse so that memory efficient methods for solving are available.

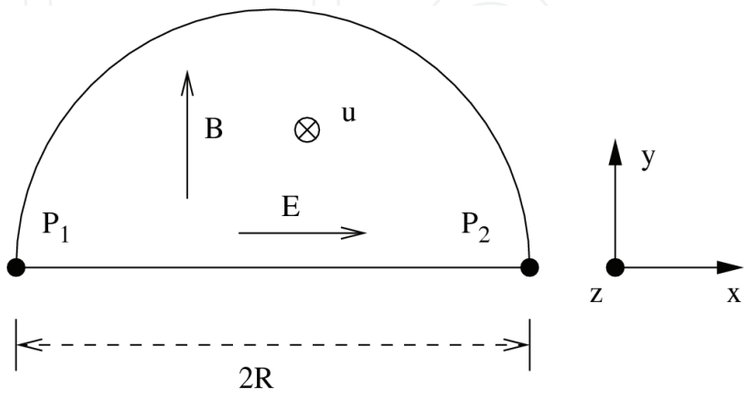

Figure 2. Sketch of evaluation model: a semicircle with radius R

The FE-technique has evolved in many engineering disciplines into software optimised for the needs of particular problems. Recently multiphysics simulations have come into focus that couples different models into one solution process. The results shown in this chapter were achieved with Comsol Multiphysics (Comsol 2005), a program that easily allows to integrate different physical phenomena and also to add further equations to the model in a mathematical form.

5. Minimum concentration

For an MI-device to work the fluid must contain mobile electric charges. Here we want to discuss the minimum requirements for water with dissolved salts. Since a certain concentration of ions also means that water conducts electrically, usually a minimum conductivity is required by the manufacturer and values are of the order of 5 µS/cm. Actually AC measurements depend on conductivity for a second reason because during measurement a current flows in the medium. When using a high impedance measurement in a static field one can assume that no current flows in the medium and only the built-up of a space charge is the limiting factor for a minimum concentration. Three sources of charge have to be considered in water:

- ions from dissolved salts,
- H^+ and OH^- ions generated by the autoprotonation reaction of water, and
- water molecules themselves, which constitute electric dipoles and can be oriented in a field to form a net polarisation charge.

It is informative to study these effects separately.

5.1 The model

The influence of the mentioned charge sources is studied on a very simple example of an infinite long circular tube with laminar flow in a homogeneous magnetic field. With radius R and maximum flow velocity u_0 the profile has the form

$$\mathbf{u} = \frac{u_0}{R^2}\left(R^2 - x^2 - y^2\right)\mathbf{e}_z\,, \tag{16}$$

where the axis of the tube is oriented along the z-axis. If we assume further that the magnetic induction of strength B_0 is along the y-axis, the high concentration limit (eq. (4)) can be solved analytically and reads

$$\varphi = B_0 \frac{u_0}{4} R^2 x\left(3R^2 - x^2 - y^2\right). \tag{17}$$

The voltage measured in an experiment corresponds to the potential difference between two points. It reaches its maximum for two points diametrically opposed in x-direction. Its value is simply

$$V_{high} = B_0 u_0 R\,, \tag{18}$$

which we call the high concentration value further on. Taking the values B_0=0.1 T, u_0=0.1 m/s, and R=1 mm we get V_{high}=50 µV.

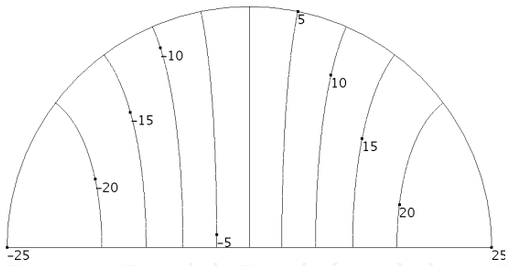

Figure 3. Equipotential lines in the high concentration limit. The grounded reference is in the centre. Values given in µV

Since the problem is constant along z a 2-D problem results. Furthermore it is symmetric and a semicircle contains all information. Figure 2 shows the relevant coordinate settings. For the high concentration solution (eq.(17)) we show the potential over the cross section as contour lines in Fig. 3.

5.2 Ions

First, we study salts that are completely dissolved, so that the generation rate in equation (13) vanishes. For each species labelled i with charge q_i equations (11,12,13) are valid separately. The model equations are in the static case:

$$\begin{aligned} \nabla\cdot\left(\mathrm{c_i q_i}\left(-\nabla\varphi+\mathbf{u}\times\mathbf{B}\right)-\mathrm{k_b T}\nabla\mathrm{c_i}\right) &= 0 \quad \mathrm{i}=1\ldots\mathrm{n} \\ -\nabla\cdot\left(\varepsilon_0\varepsilon_\mathrm{r}\nabla\varphi\right) &= \sum \mathrm{q_i c_i}. \end{aligned} \tag{19}$$

The magnetic induction and temperature are assumed to be homogeneous. For n different types of ions the system is represented by n+1 degrees of freedom and as many equations. The first equations state essentially conservation of the particle numbers. Note that in the static case the particle mobilities do not appear in the equations. The assumption here is that the system relaxes to the equilibrium fast enough.

Since ions species with the same charge lead to identical equations we treat the concentration variables c_i in equation (19) as the accumulation of all ions having the same charge. Our model example is simplified in another respect, because only anions and cations with elementary charge are included and hence only two concentration variables c_+ and c_- remain (where q_0 denote the elementary charge):

$$\begin{aligned} \nabla\cdot\left[\mathrm{c_+ q_0}\left(-\nabla\varphi+\mathbf{u}\times\mathbf{B}\right)-\mathrm{k_B T}\nabla\mathrm{c_+}\right] &= 0 \\ \nabla\cdot\left[-\mathrm{c_- q_0}\left(-\nabla\varphi+\mathbf{u}\times\mathbf{B}\right)-\mathrm{k_B T}\nabla\mathrm{c_-}\right] &= 0 \\ -\nabla\cdot\varepsilon_0\varepsilon_\mathrm{r}\nabla\varphi &= \mathrm{q_0}\left(\mathrm{c_+}-\mathrm{c_-}\right). \end{aligned} \tag{20}$$

The model can be extended to ions with higher order charge ions with no difficulties.

The solution for this system of equations is depicted in fig. 4 (solid line) as a plot of the voltage across the diameter in dependence on the salt concentration. We state that above a concentration of 10^{14} 1/m^3 the high concentration limit is attained. This is as we will see later five orders of magnitude above the concentration of the H^+ and OH^- ions in pure water.

5.3 Dipoles

The water molecule features an electric dipole moment and for this reason is oriented in an electric field. In a nonhomogeneous electric field this leads to a net polarisation. The

susceptibility of a material $\varepsilon_0(\varepsilon_r\text{-}1)$ measures its ability to create such a polarisation charge. It can be shown from thermodynamics (Feynman et al. 1966) that

$$\rho_{\text{pol}} = -\nabla \cdot \varepsilon_0 (\varepsilon_{\text{r}} - 1)\mathbf{E}. \tag{21}$$

Usually this polarisation charge does not show up explicitly in the equations because it is automatically included in the macroscopic Maxwell equations in the form of the relative permittivity. When a magnetic induction is present and the medium moves, equation (21) has to be extended to

$$\rho_{\text{pol}} = -\nabla \cdot \varepsilon_0 (\varepsilon_{\text{r}} - 1)(\mathbf{E} + \mathbf{u} \times \mathbf{B}), \tag{22}$$

which is discussed by Simonyi (1979) in more detail and derived by Engl (1960) for the electromagnetic flow meter. This gives rise to an augmented form of Poisson's equation:

$$-\nabla \cdot \varepsilon_0 \varepsilon_{\text{r}} \nabla \varphi = \rho_{\text{mac}} - \nabla \cdot \varepsilon_0 (\varepsilon_{\text{r}} - 1)(\mathbf{E} + \mathbf{u} \times \mathbf{B}). \tag{23}$$

At first let us note that in the case when the liquid contains no other mobile charges, equation (23) is equivalent to equation (4) with the potential being reduced by a factor of $(\varepsilon_r\text{-}1)/\varepsilon_0$. In water, which has a relative permittivity of 80, this means that the MI-voltage reaches 79/80≈99% of the high concentration value, even when there are no dissolved ions at all.

For demonstration purposes we repeat the calculations from subsection 5.2 for a liquid with polarisation effects that has ε_r=3, which is easier to discriminate in fig. 4 (where it is shown as dashed line) than water. The transition to the high concentration limit is at the same concentration value but at lower concentrations the MI-effect is never zero.

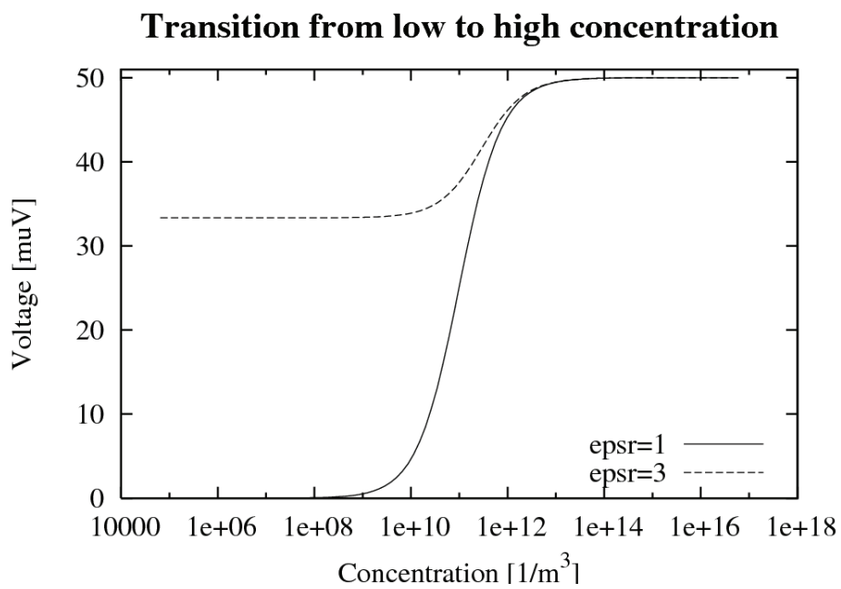

Figure 4. Transition for a solution with monovalent ions in a hypothetical liquid with no polarisation (ε_r=1) and with polarisation effects (ε_r=3)

5.4 Autoprotonation

Even pure water contains ions which are H^+ and OH^- and originate from the autoprotonation reaction of water

$$H_2 0 \leftrightarrow H^+ + OH^-. \tag{24}$$

In this context we do not want to discuss the nature of these ions and in which embodiment they are dissolved in water, but we treat all quantities (concentration, mobility, ...) as effective quantities for a positive and a negative charge respectively. In fact these effective properties are measured in experiments; for the effective mobility Atkins (1988) reports the values

$$\begin{aligned} \mu_{H^+} &= 2.26 \quad 10^{12}\,\mathrm{m}^2/\mathrm{Js} \\ \mu_{OH^-} &= 1.29 \quad 10^{12}\,\mathrm{m}^2/\mathrm{Js} \quad . \end{aligned} \tag{25}$$

Two aspects have to be taken into account. First, the generation rates (see eq.(13)) are equal for the two ion species because they are created or destroyed in pairs. Second, in a chemical equilibrium the mass action law states that the product of the two concentrations is constant

$$c_{H^+} c_{OH^-} = K^2 \tag{26}$$

with K = 10^{-7} mol/l = 6.06 10^{19} 1/m^3. The value *K* is the concentration of the ions in pure water or at pH=7. As a consequence of mass action only one concentration variable is independent. A convenient parametrisation is the choice

$$\begin{aligned} c_{H^+} &= K e^{\psi} \\ c_{OH^-} &= K e^{-\psi} \quad . \end{aligned} \tag{27}$$

The new degree of freedom Ψ is related to the pH-value in chemistry. When applying the drift-diffusion model (equations (11) and (13)) to the concentration variables for a nonpolarisable medium we get the system of equations

$$\begin{aligned} \mu_{H^+} \nabla \cdot \left[c_{H^+} q_0 \left(\mathbf{E} + \mathbf{u} \times \mathbf{B} \right) - k_B T \nabla c_{H^+} \right] &= G \\ \mu_{OH^-} \nabla \cdot \left[- c_{OH^-} q_0 \left(\mathbf{E} + \mathbf{u} \times \mathbf{B} \right) - k_B T \nabla c_{OH^-} \right] &= G \\ - \nabla \cdot \varepsilon_0 \varepsilon_r \nabla \varphi &= q_0 \left(c_{H^+} - c_{OH^-} \right) \end{aligned} \tag{28}$$

After elimination of the generation rate and using the Ψ variable, the following equations remain

$$\begin{aligned} \nabla \cdot \left(\mu_{H^+} e^{\psi} + \mu_{OH^-} e^{-\psi} \right) \left(\mathbf{E} + \mathbf{u} \times \mathbf{B} - \frac{k_B T}{q_0} \nabla \psi \right) &= 0 \\ \nabla \cdot \varepsilon_0 \mathbf{E} &= q_0 K \left(e^{\psi} - e^{-\psi} \right) \end{aligned} \tag{29}$$

Only the ratio of the mobilities exerts influence in this equation. We want to approximate these equations further. For small values of Ψ the exponential functions can be expanded in lowest order, giving

$$\nabla \cdot \left(\mu_{H^+} + \mu_{OH^-}\right)\left(\mathbf{E} + \mathbf{u} \times \mathbf{B}\right) = 0 \qquad (30)$$

$$\nabla \cdot \varepsilon_0 \mathbf{E} = 2q_0 K \Psi \quad .$$

We see that this approximation results in the high concentration limit (first equation), which can be solved analytically for the model problem (see eq. (17)). The second equation can also be solved analytically:

$$\Psi = \frac{u_0 B_0 \varepsilon_0}{R^2 q_0 K} = 3.67 \quad 10^{-8} \frac{1}{m} \quad x \qquad (31)$$

Hence for the sizes in question (centimetre range) the approximation is justified and, hence, the use of the high concentration limit.

5.5 Consequences

The main result of the study of water including the effects of dissolved salts, polarisation of the water molecule, and autoprotonation shows that dissolved salts are not needed for the built-up of a magnetic inductive potential. The electric and chemical properties of water alone produce sufficient charge density for the (previously known) high concentration limit. This can already be seen in the fact that the transition found in subsection 0 occurs at a concentration below 10^{14} $1/m^3$ which is five orders of magnitude below the concentration of H^+ and OH^- in pure water. Adding up the different effects (salt ions, polarisation, autoprotonation) justifies the use of the high concentration limit for water in all cases.

One important constraint has to be mentioned here concerning technical implementations. In currently available devices an AC magnetic field is used and during measurement an electric current is flowing in the medium, thus requiring a conductive medium. This must be considered an additional reason for the need for a minimum conductivity (and minimum salt concentration at the same time). In a static measurement with high-ohmic amplifiers no current flows in the medium and the minimum concentration is no longer needed.

Another interesting consequence derives from the polarisation effect that is not only present in water but also in other liquids like oil or petrol. These liquids are not conducting under normal circumstances. Therefore the electromagnetic flow meter can be used in an even wider range of applications as previously known.

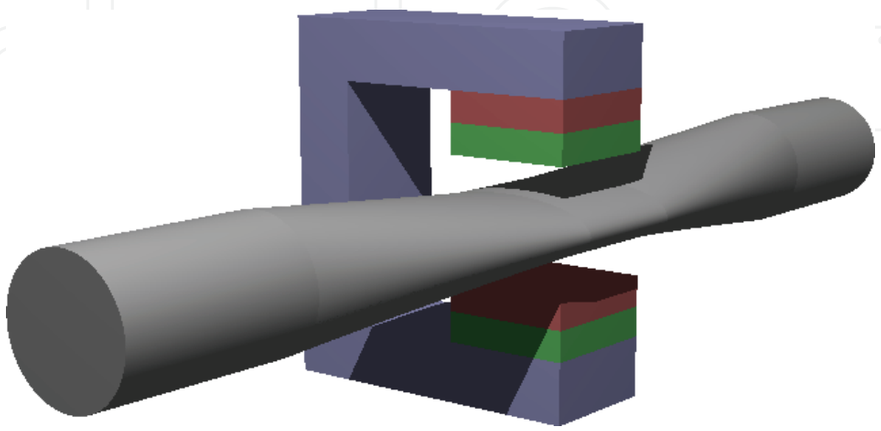

Figure 5. Model for geometry optimisation

6. Geometric shape optimisation

The design of a complete electromagnetic flow meter requires the solution of a coupled system. The results of section 5 justify the application of the high concentration limit and the model comprises equations of magnetostatics (eq. (9)), fluid dynamics (eq.(1,2)), and the magnetic-inductive effect (eq. (4)). We apply this system of equations to an optimisation problem. The main idea is as follows: the sensor region usually has a circular cross section but can also have other shapes, for instance an ellipse. The geometry influences the flow and in consequence the electric output of the sensor. Also the magnetic system changes because the magnet poles can be placed closer to each other. Figure 5 shows the model as it was used in the calculations. In the sensitive region the cross section is quenched to an elliptic shape with a smooth transition to circular pipes that are attached to the sensor. The poles of the magnet are placed close to the pipe and a return yoke is included for efficient utilisation of the magnetic field. The electric connections are not shown in this figure but in the calculations capacitive coupling is used. These contacts must be large for an efficient electric coupling and span an angle of 150^{o}.

The shape of the cross section is parametrised such that the ellipse has the half axes ($R\beta(1-\alpha)$,$R/(1-\alpha)$), where the parameter α applies to the shape of the ellipse, β changes the size, and R is the equivalent radius of a circular tube. The parameter α is chosen such that at the value zero the circle is recovered as the cross section. The area of the cross section is $\pi\beta R2$. The goal of the optimisation is highest sensitivity and two constraints must be met:

- The pressure drop shall be the same as for a straight tube.
- The sensor is nonlinear but should not deviate from the ideal linear case too much.

6.1 Model size

Naturally the results of such an optimisation depend on the material parameters, geometric sizes and flow conditions. So numeric results should be taken as an example and the main objective of this section is the methodology. The application field in the numeric case is water at room temperature in tubes with 1 cm diameter in a flow range of 0-4 m/s medium flow velocity. A target velocity is fixed at 1 m/s, for which the pressure drop is adjusted, so that the flow meter is neutral in the pipe circuit. For other velocities the flow meter is operational but the pressure drop differs. The values mentioned must be considered as one example: the methodology can be employed to other cases in the same way. The relevant properties of water are

- density: 1000 kg/m^3
- viscosity: 8.54 10^{-4} Pa s
- relative dielectric constant: 80.

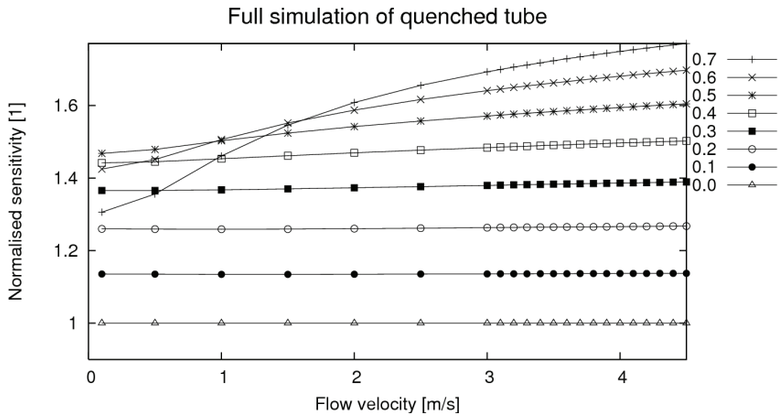

Figure 6. Sensitivity of quenched flow meter for different α-values

6.2 Pressure drop

The first constraint is equivalent to the demand that the flow meter should have no disturbing effect on the flow circuit. In fact if the tube is quenched the flow resistance of the tube increases. Therefore enlarging the area (via parameter β) neutralises the effect. In order to find the compensation, NS equations are solved for various parameters. For each given parameter value α the corresponding β-value can be found such that the pressure drop equals that of a straight tube. It is instructive to convert this dependence into polynomial form

$$\beta(\alpha) = 1 + 0.922\alpha^2 + 0.698\alpha^4 + 1.618\alpha^6 \ . \tag{32}$$

This compensation function depends on the velocity; in this case the target velocity is 1 m/s.

6.3 Magnetostatics

The calculation of the magnetic field follows the approach of a scalar magnetic potential as outlined ins subsection 3.3. For the permanent magnet we assume a constant magnetisation and the ferromagnetic material of the return yoke is simulated by a very large relative permeability.

6.4 Simulations

Using this pressure compensated system we perform the three simulation steps (magnetostatics, fluid dynamics, and electrostatics) needed to establish the magnetic-inductive response. Figure 6 shows the sensitivity $S=V/u_0$ for different deformation parameters. For values $\alpha>0.5$ we judge that the nonlinearity is unacceptably large. This depends in fact on the envisaged application.

In the next step we compare the sensitivity for different values of the deformation parameter at the target velocity u_M. We get the result displayed in fig. 7. The optimal configuration, if higher nonlinear behaviour can be tolerated, is at $\alpha=0.55$, but keeping the previously outlined limit the optimal shape is with $\alpha=0.5$. The improvement in the magnetic-inductive effect compared to the standard configuration is between 45% and 50%.

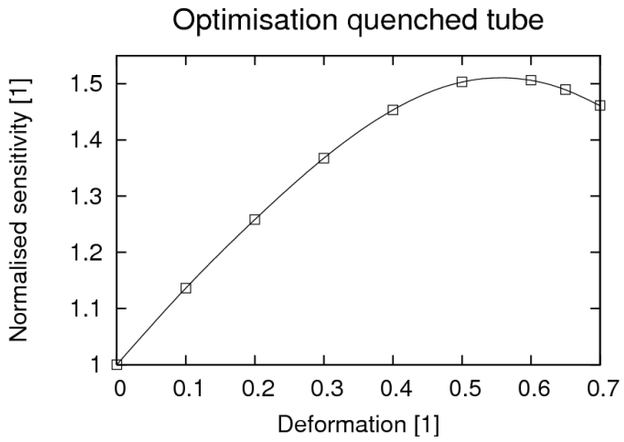

Figure 7. Sensitivity at 1 m/s with optimum at α=0.55

6.5 Methodology and efficient calculations

Since for an optimisation problem many single computations of the model are needed an efficient methodology is important. The design of a flow sensor supported by FE-simulations is done in the following steps. We start with a given standard configuration, like having a circular cross section, the operating range in terms of a velocity interval and the main operating velocity u_M.

1. A parametrised CAD-model of the flow sensor is created with a deformation parameter α such that for α=0 the standard configuration is met. A second parameter β is used to scale the area. The inlet and outlet tubes with circular cross section and appropriate connection to pipes are included. The parametrised CAD model also adjusts the magnet's position to the deformed sensor device.
2. In a first set of FE-simulation at the velocity u_M the NS equations are solved for ranges of the parameters α and β. The goal is to find the function $\beta(\alpha)$ that adjusts the area of the cross section, so that the pressure drop at each value of α is that of the standard configuration.
3. For each parameter value α the magnetic field is computed by solving the magnetostatic equation for the adjusted positions of the magnet.
4. The NS equations are solved for the entire velocity range in the compensated model and the resulting magnetic inductive potential is computed.
5. The results are first analysed for linearity. That means for each value α the magnetic-inductive response (the voltage V at the capacitive contacts) is examined. Depending on the needs of the applications an upper bound for the allowed α-values is established.
6. Comparing the sensitivity $S=V/u_0$ at u_M for all α gives the optimal parameter value.

6.6 Geometric symmetry

The different physical models have their own symmetries and an efficient simulation employs these symmetries in the way that the domain is restricted and the solution is mirrored. This technique reduces the number of degrees of freedom and in consequence the time and memory requirement for a single simulation considerably. Figure 8 shows the minimal model with a tube that is oriented in z-axis. The flow field has a fourfold symmetry

and the NS equations are only solved in a quarter. The full solution result can be constructed by mirroring at the planes x=0 and y=0. Next, the magnetic subsystem also has a fourfold symmetry but along the x-axis and the solution is mirrored at z=0 and y=0. Because the right hand side of the MI-equation is determined form the flow field and magnetic field, the electrostatic model has a twofold symmetry with mirror plane y=0.

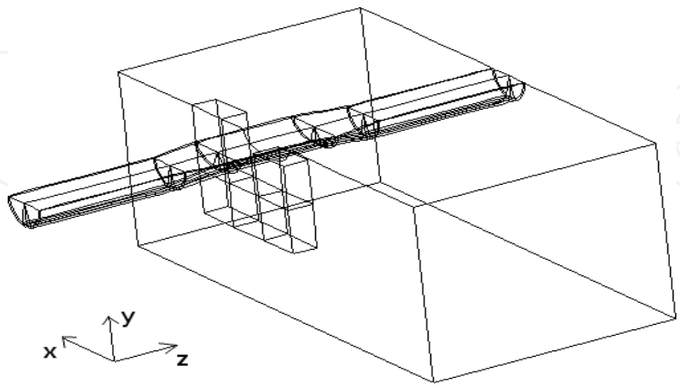

Figure 8. Geometric model for simulation

6.7 Conclusions

A novel and simple improvement in the configuration of the magnetic inductive sensor allows an increase of the measured voltage, and therefore the sensitivity, of about 50%. In the new configuration the cross section of the measuring unit is not circular any more but, in the present example, elliptical. This increase in sensitivity can be explained by two effects:

- The fluid flow has a different pattern, which induces a larger space charge density and in consequence a higher voltage.
- Due to the deformation of the tube the magnet pole faces can be placed closer to each other and the magnetic field is exploited more efficiently.

The potential use of the increase in the MI effect is that sensors can be built smaller or with higher sensitivity. The main drawback is that, compared with a straight tube, the MI response is not linear any longer. The design method, however, gives full control over the limits of the nonlinearity. Also the nonlinear behaviour is such that the response is even larger than one would expect with a linear sensor. That means that even stronger signals can be achieved if nonlinear behaviour can be tolerated.

7. Turbulent fluctuations

Turbulence is a phenomenon in fluid dynamics of great attention in research and application. It corresponds to solutions of the (nonlinear) NS-equation that are unsteady and exhibit chaotic behaviour. In contrast, laminar flow is represented by stable solutions of the stationary NS equations. Stability in this respect means that small perturbations to the flow are damped and disappear with time. The flow can be characterised by the dimensionless Reynolds number

$$\mathrm{Re} = \frac{\rho \mathrm{u}_0 \mathrm{L}}{\mu}, \tag{33}$$

where u_0 and L are characteristic velocity and length scale values, respectively.

The NS equations can be transformed into a nondimensional form and the Reynolds-number remains as the only parameter (Spurk & Aksel 2006):

$$\dot{\mathbf{u}} + (\mathbf{u} \cdot \nabla)\mathbf{u} = -\nabla p + \frac{1}{\mathrm{Re}} \Delta \mathbf{u} \,. \tag{34}$$

This form of the NS equations has the advantage to demonstrate that different fluids obey the same laws parametrised by the Reynolds-number. The necessary transformations are:

$$\begin{aligned} \mathbf{u} &\rightarrow u_0 \mathbf{u} \\ x &\rightarrow Lx \\ p &\rightarrow L u_0^2 p \\ t &\rightarrow \frac{L}{u_0} t \quad . \end{aligned} \tag{35}$$

Laminar flow is characterised by Reynolds-numbers smaller than 2000-3000. At higher Reynolds-numbers the inertia term exceeds friction in influence and small perturbations are amplified. In a fully developed flow the field quantities fluctuate in a chaotic form. In many practical applications only mean values are of interest, which is reflected in CFD by models for the mean flow velocity (Reynolds-average Navier Stokes, RANS). One popular model for high Reynolds-numbers is the *ke*-model which adds two auxiliary properties (turbulent kinetic energy and dissipation rate) to the equation system. The literature on this subject is rich, e.g., see Eggels (1994), Launder et al. (1975).

The consequence of turbulence for the magnetic-inductive flow meter is that the fluctuations of the flow lead to fluctuations in the potential and in the measured voltage. When the average voltage is evaluated, the *ke*-model replaces the NS equations in the modelling and the electric potential and field are understood as average quantities. In the following we want to examine the fluctuations themselves and aim to find the amplitude of these voltage fluctuations and for this reason the *ke*-model cannot be applied. The goal is to examine the strength of these amplitudes and to establish the dependence of the amplitude from the volume flow in the tube. These results turn out to be convincing that the amplitude of the voltage fluctuations can be used as a measure for the volume flow.

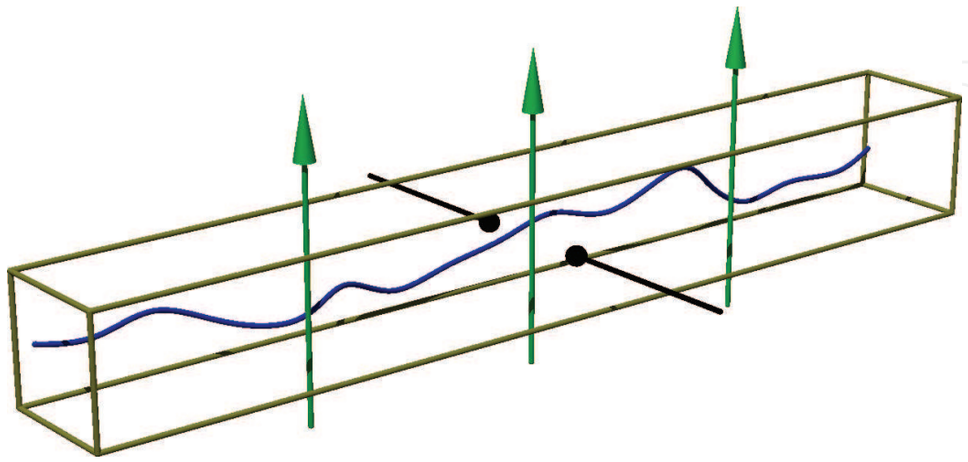

Figure 9. Model for LE-simulations: a tube with square cross section and a homogeneous magnetic field. Blue line indicates a possible turbulent flow line

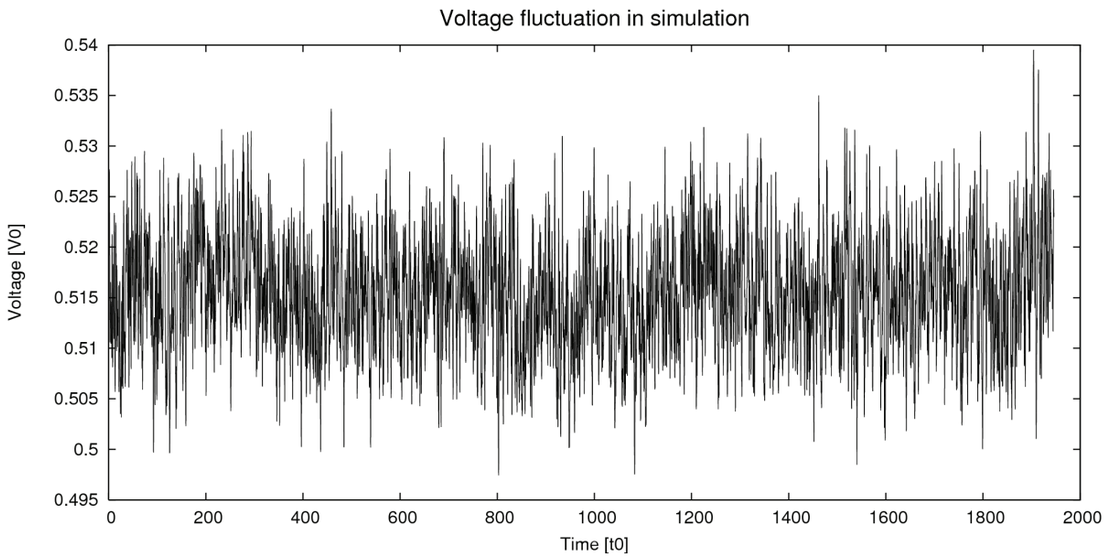

Figure 10. Voltage fluctuation of MI flow meter in large eddy simulations at Re=14000. The amplitude is about 5% of the mean value and therefore large enough to be measured

For realistic simulation of turbulent phenomena including fluctuations small time and space scales have to be resolved. Here the FE-method demands too many computer resources and the Finite-Difference (FD) method is preferred. Since the FD method calls for a regular grid only simple geometries can be treated.
Whereas the so called *direct numerical simulation* use the plain NS equations, the large-eddy simulations only treat large scale turbulences and suppress small eddies, so the resource requirements are less severe.
To test the influence of turbulence on the electromagnetic flow meter we describe FD simulations that calculate the amplitude of a MI signal in a straight tube with square cross section (fig. 9). The model has a homogeneous magnetic field (green arrows) and pointlike galvanic electrodes (black lines). The blue line shows the stream line of one fluid particle.

7.1 Large-eddy (LE) simulation

We employ the large-eddy model in the way it is described in the reference by Eggels (1994). The governing equations follow from the NS equations by applying a spatial filter operator. This filter averages the fluctuating velocity components in a small environment around a point and has the effect to suppress small eddies (called sub-grid scale) and preserve larger ones (grid scale).
The governing equations for the LE-model are essentially the the NS-equation for the filtered unknowns **u** and *p*. In dimensionless form they read:

$$\begin{aligned} \dot{\mathbf{u}} + (\mathbf{u}\cdot\nabla)\mathbf{u} &= -\nabla p - \nabla P + \frac{1}{\mathrm{Re}}\Delta\mathbf{u} - \nabla\tau \\ \nabla\cdot\mathbf{u} &= 0. \end{aligned} \tag{36}$$

An additional quantity, the LE-stress tensor τ, must be introduced to model the subgrid eddies. All detailed information about these eddies is lost in the averaging process but heuristic models can be formulated to account for their influence on the main flow and this

influence is expressed in the stress tensor τ. Here the pressure gradient is split in two parts: on one side the gradient of *P*, which is constant in space for a straight tube and drives the flow through the tube. On the other side the unknown part *p* ensures incompressibility.
In the Smagorinsky model the LE-strain is found from the strain tensor (Denev et al. 2003)

$$\mathrm{S} = \left(\nabla \otimes \mathbf{u}\right) + \left(\nabla \otimes \mathbf{u}\right)^{\mathrm{t}} \tag{37}$$

assuming that the stress has the form

$$\tau = -\mathrm{l}_{\mathrm{mix}}^{2} \sqrt{2\,\mathrm{trace}\left(\mathrm{S}^{2}\right)}\,\mathrm{S} \tag{38}$$

i.e., the LE-stress has the anisotropy of the strain and the effective LE-viscosity is proportional to the magnitude of the strain. The mixing length l_{mix} is related to the average grid size

$$\mathrm{l}_{\mathrm{grid}} = \sqrt{\delta \mathrm{x}^{2} + \delta \mathrm{y}^{2} + \delta \mathrm{z}^{2}} \tag{39}$$

by $l_{mix}=c_s\, l_{grid}$, where c_s is Smagorinsky's constant. Its value is open to debate but values in the range 0.1...0.2 are usually chosen. In this work c_s=0.16.
As boundary conditions homogeneous Dirichlet *no-slip* conditions are applied on the walls of the tube for all velocity components and Neumann conditions for the pressure *p*. In axial direction the model in principle requires an infinitely long tube. Considering the fact that in streamline direction the fluctuations at two points are not correlated any more if the distance is large enough, one can apply periodic boundary conditions to a tube of finite length. This can be regarded as a feedback loop of the outlet to the inlet. If the length of the tube is larger than the correlation length no artefacts are introduced by this procedure. Eggels (1994) reported that a length of at least five times the diameter of the tube is sufficient. In the present results the length is eight time the edge length of the cross section.
Usually LE simulations are performed at constant pressure gradient, which implies a fluctuating mean flow because the resistance of the tube depends on the turbulent activity, which is fluctuating by nature. We force a constant mean flow (which is important for flow-metering) by allowing the pressure gradient to vary in time and evaluate the integral

$$\partial_{\mathrm{x}} \mathrm{P} \left|\Omega\right| = \int \left(\frac{1}{\mathrm{Re}} \Delta \mathrm{u}_{\mathrm{x}} - \left(\nabla \cdot \tau\right)_{\mathrm{x}} \right) \; \mathrm{dx}^{3} \tag{40}$$

at every time step. The integral follows from eq. (36) by integrating the stream-wise component over the tube volume Ω and applying boundary conditions. The other components of the pressure gradient are zero. In reference Denev et al. (2003) the flow velocity is corrected after each time step to ensure constant global mass flow rate.
The magnetic inductive potential is solved at each time step using equation (4) in a post-processing step. Similar LE-simulation were reported by Boersma & Nieuwstadt (1999) but only for one Reynolds-number. Since the dependence on flow rate is our main interest we repeated calculations on a 265 x 65 x 65 grid for a pipe of length 8 over a unit square cross section with sufficient accuracy.
As a typical example we show the magnetic inductive voltage fluctuation of a simulation at Re=14000 in fig. 10. The amplitude of the fluctuation is about 15% of the mean value. This, in our belief, is high enough to be measured reliably in experiments.

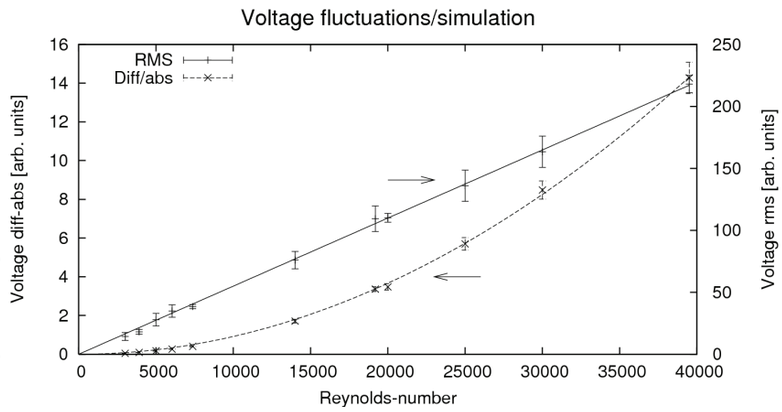

Figure 11. Amplitude of voltage fluctuations of an electromagnetic flow meter in dependence on Reynolds-number in the simulation. The analysis as root-mean-square shows linear behaviour, where the amplitude of the differentiated signal has quadratic dependence

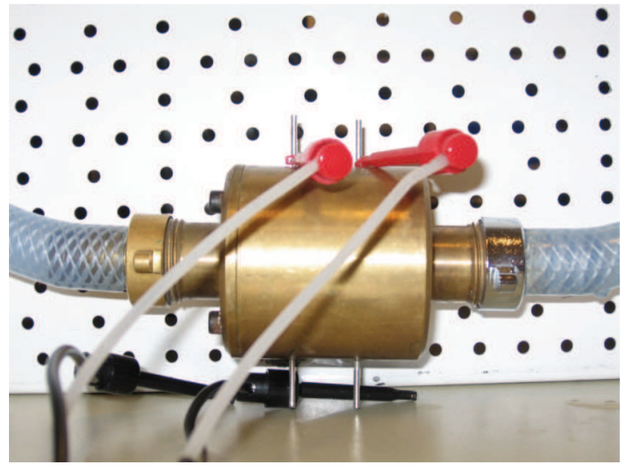

Figure 12. Experimental set-up for the measurement of the turbulent flow meter

Further analysis of the experimental data has been undertaken in two ways:

- as statistical root-mean-square of the voltage and
- as the average of the modulus of the time-differentiated signal.

The averaging is done for packages of sampling points together with the calculation of error intervals. The results are shown in fig. 11 with a maximum Reynolds-number of 40,000, which corresponds to a mean flow velocity of 3.8 m/s for water at room temperature and a tube with 1 cm edge length. We observe that the root-mean-square linearly depends on the Reynolds-number while the amplitude of time-differentiated is a quadratic function of the Reynolds-number and hence of the mean flow velocity. The consequence of the monotonous dependence of the noise on the flow rate suggests that the amplitude can be employed to measure the mean flow. Since the error of the time-differentiated signal is small, the type of evaluation is preferred.

At low flow rates when the flow is laminar this type of flow sensor cannot be used. In the present parametrisation where u_0 is the mean flow velocity and L the edge length of the cross section the flow is laminar below a Reynolds number of 3000.

7.2 Experimental verification

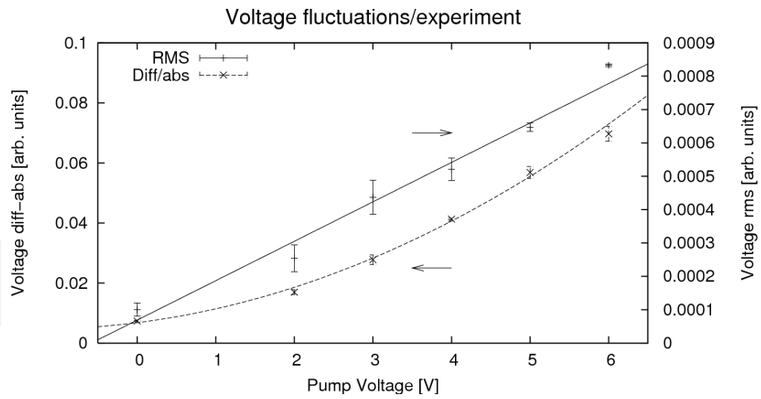

Figure 13. Amplitude of voltage fluctuations of an electromagnetic flow meter in dependence on the pump voltage (proportional to the mean flow velocity) in the experiment. Simulation and experiments agree in the functional dependence of the amplitudes

Briefly we want to show that the LE-simulation that we have presented can be verified in experiments. The measurements were performed with the simple set-up shown in fig. 12 using tap water at room temperature. The water circuit is constructed with plastic tubes with inner radius of 13 mm and a voltage driven pump. In the actual sensitive region the cross section is narrower (75 mm^2) and the magnetic induction from permanent magnets is at maximum 0.5 T. Using this small set-up the results in fig. 13 are measured. The analysis is done in the same two techniques as for the simulations. The dependence on the mean flow rate is the same that was found in the calculations.
Measuring the amplitude of these fluctuations is hampered by other noise sources coming from the electric circuit, electrochemical double layers, and radiation. Some of these noise sources are flow independent and explain the noise amplitude at zero flow. Of the flow dependent noise the agreement between simulation and experiment suggests that indeed the turbulence explains a major part of the noise.

7.3 Optimal placing of contacts

The optimal placement of the two contacts in a conventional MI-flow meter is such that the contacts are arranged perpendicularly to the magnetic filed. The voltage reaches its maximum in this configuration. For a flow meter working on the turbulent paradigm the optimal position differs as can be deduced from fig. 14. It shows in a colour scale (blue to red) the amplitude of the fluctuations (in the root-mean-square measure). The reference contact is fixed at one the standard positions, i.e., at the centre of the blue spot. All points of the surface are sampled to measure in the simulation the noise amplitude relative to the reference point and the result plotted in the figure. It turns out that the fluctuation is strongest if the second contact is placed in the axis of the magnetic field, i.e., at an angle of 90^o degrees with the reference. In this respect the LE-simulation foresees future experiments and helps to optimise a new flow meter principle.

7.4 Conclusion

A new measurement principle relying on the turbulent nature of liquid flow in a pipe is verified with numerical simulations. In fact, fluctuations in the flow lead to fluctuations in

the pick-up voltage and the amplitude of the these fluctuations depends monotonously on the mean flow and can therefore be used as measure for the mean flow. The functional dependence of the signal is the same for experiments and simulations. The simulation also shows that the strength of the signal is high enough to be measured. This fact strongly supports the view point that the flow dependent fluctuations in the experiment are explained by the turbulent activity.

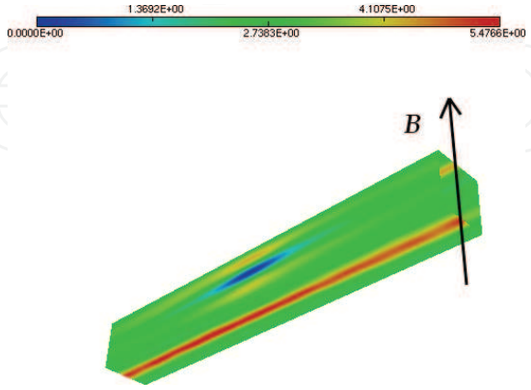

Figure 14. Turbulent flowmeter: distribution of amplitude of fluctuations on the surface. The reference point is in the centre of the blue spot, the optimal position of the second contact in the area

8. Summary

Numerical simulations are used in sensor design in an advance fashion. We have shown for the electromagnetic flow meter that basic physical and electrochemical phenomena can be modelled such that engineers can make forecasts about new generation devices.

The first concrete result, that we demonstrated, concerns the minimum concentration of dissolved salt ions needed for a magnetic inductive flow meter to work. Until now industrial applications required a minimum conductivity. Using basic models for all possible mobile charges (ions from dissolved salts, autoprotonation of water, and polarisation effects) we can show that even in pure water and other polarisable liquids the MI-effect is strong enough to be measured. The possible impact on technology is enormous: the application range of electromagnetic flow meters is wider than it was believed before. The trade-off is that high-ohmic electronic circuits must be implemented because no electric current can flow in the medium. But modern electronic devices offer this possibility.

Second, we can use the Finite-Element technique for geometric shape optimisation. Naturally, optimisation using actual prototypes can be tedious and computations allow shorter design cycles. On the other side the simulation of the MI flow meter demands software that easily and effectively handles multiphysics problems like for instance Comsol Multiphysics does. In the detailed example we improve the sensitivity of an electromagnetic by 50% solely by changing the cross section of the measuring tube.

The third and final result treats turbulent flows and requires direct numerical simulations or large-eddy simulations. These techniques used to be reserved to supercomputers but with small server becoming faster smaller departments can investigate turbulences on small time and length scales. This leads to the following new principle for flow metering. Turbulent flow is intrinsically unsteady and flow quantities fluctuate. These fluctuations lead to fluctuations in

the voltage measured by an MI device. We investigate the amplitude of the fluctuations as a function of the Reynolds-number, i.e., the flow rate. We find a monotonous dependence, that is sufficiently confirmed in experiments, and propose to use this amplitude to measure the flow rate. The simulations are also used to optimise the placement of the pick-up electrodes with the astonishing outcome that the electrodes are best placed at an angle of 90^{o}.
We note that these results can be obtained using advanced software tools and moderate computer resources. There simulations based on fundamental physical properties are in reach of every engineering department.

9. References

Atkins P. W. (1988), *Physikalische Chemie*, VCH, Weinheim

Boersma B.J. & Nieuwstadt F.T.M. (1999). On the Electric Potential Induced by a Homogeneous Magnetic Field in a Turbulent Pipe Flow. *Flow, Turbulence and Combustion* Vol. 62, 29-51. ISSN 1386-6184

Ciarlet P.G. (1978) *The Finite Element Method for Elliptic Problems*, North-Holland, Amsterdam.

Comsol AB (2005). *Comsol Multiphysics Modelling Guide*; Version Sep. 2005, Stockholm

Denev J.; Frank Th. & Pachler K. (2003). Large Eddy Simulation of Turbulent Square Channel Flow Using a PC-Cluster Architecture, In: *4th Intl. Conf. on Large-Scale Scientific Computations*, 363-370.

Eggels J. G. M. (1994). *Direct and Large Eddy Simulation of Turbulent Flow in a Cylindrical Pipe Geometry,* Ph.D. thesis Technische Universiteit Delft, Delft.

Eggels J.G.M.; Unger F.; Weiss M.H.; Westerweel J.; Adrian R.J.; Friedrich R. & Nieuwstadt F.T.M. (1994). Fully developed turbulent pipe flow: A comparison between direct numerical simulation and experiment. *Journal of Fluid Mechanics*, Vol. 268, 175-209.

Eggels J.G.M.; Westerweel J.; Nieuwstadt F.T.M. & Adrian R.J. (1993). Direct numerical simulation of turbulent pipe flow. *Applied Scientific Research. Vol.* 51, 319-324.

Engl W. (1960). Relativistische Theorie des induktiven Durchflussmessers, *Archiv für Elektrothechnik*, Vol. 46, 173-189

Fiedler O. (1992). *Strömungs- und Durchflußmeßtechnik*, R. Oldenbourg, München

Feynman R. P., Leighton R. B, Sands M. (1966). *The Feynman Lectures on Physics*, Vol. 2, Addison-Wesley

Hamann C. H. & Vielstich W. (2005). *Elektrochemie*, 4th edition, Wiley-VCH

Launder B. E.; Reece G. J. and Rodi W. (1975). Progress in the Development of a Reynolds-Stress Turbulent Closure. *Journal of Fluid Mechanics*, Vol. 68, No. 3, 537-566.

Schommartz G. (1974) *Induktive Stömungsmessung*, VEB Verlag Technik, Berlin

Simonyi K. (1979). *Theoretische Elektrotechnik*, VEB Deutscher Verlag der Wissenschaften, Berlin

Shercliff J. A. (1954), Relation between the velocity profile and the sensitivity of electromagnetic flowmeters. *Journal of Applied Physics*. Vol. 25, 817-818

Stange G. (2002) *Verfahren zur Messung eines ein Messrohr durchströmenden Mediums*, German Patent

Spurk J. H. & Aksel N. (2006) *Strömungslehre: Einführung in die Theorie der Strömungen*, 6th edition, Springer

Williams E. J. (1930). The induction of electromotive forces in a moving liquid by a magnetic field, and its application to an investigation of the flow of liquids. *Proceedings of the Physical Society* Vol. 42, 466-478

Zienkiewicz O. C. & Taylor R. L. (1989). *The finite element method, 4th edition*, McGraw-Hill, London

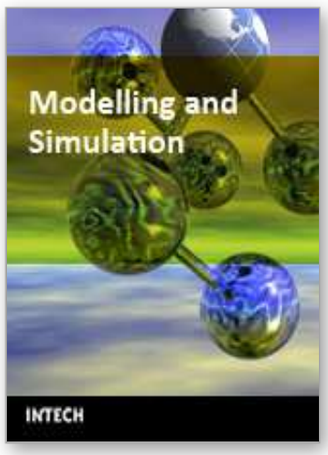

Modelling and Simulation

Edited by Giuseppe Petrone and Giuliano Cammarata

ISBN 978-3-902613-25-7
Hard cover, 688 pages
Publisher I-Tech Education and Publishing
Published online 01, June, 2008
Published in print edition June, 2008

This book collects original and innovative research studies concerning modeling and simulation of physical systems in a very wide range of applications, encompassing micro-electro-mechanical systems, measurement instrumentations, catalytic reactors, biomechanical applications, biological and chemical sensors, magnetosensitive materials, silicon photonic devices, electronic devices, optical fibers, electro-microfluidic systems, composite materials, fuel cells, indoor air-conditioning systems, active magnetic levitation systems and more. Some of the most recent numerical techniques, as well as some of the software among the most accurate and sophisticated in treating complex systems, are applied in order to exhaustively contribute in knowledge advances.

INTECH
open science | open minds

InTech Europe
University Campus STeP Ri
Slavka Krautzeka 83/A
51000 Rijeka, Croatia
Phone: +385 (51) 770 447
Fax: +385 (51) 686 166
www.intechopen.com

InTech China
Unit 405, Office Block, Hotel Equatorial Shanghai
No.65, Yan An Road (West), Shanghai, 200040, China
中国上海市延安西路65号上海国际贵都大饭店办公楼405单元
Phone: +86-21-62489820
Fax: +86-21-62489821

IntechOpen